Applied Physics Express

LETTER

Nonlinear optical properties of chalcogenide glass waveguides fabricated by hot melt smoothing and micro-trench filling

Applied Physics Express 13, 042005 (2020)
https://doi.org/10.35848/1882-0786/ab7e42

LETTER

Nonlinear optical properties of chalcogenide glass waveguides fabricated by hot melt smoothing and micro-trench filling

Renduo Qi[1], Wei Zhang[1,2,3*], and Yidong Huang[1,2,3]

[1]Beijing National Research Center for Information Science and Technology (BNRist), Beijing Innovation Center for Future Chips, Electronic Engineering Department, Tsinghua University, Beijing 100084, People's Republic of China
[2]Frontier Science Center for Quantum Information, Beijing 100084, People's Republic of China
[3]Beijing Academy of Quantum Information Sciences, Beijing 100193, People's Republic of China

*E-mail: zwei@tsinghua.edu.cn

Received February 28, 2020; accepted March 9, 2020; published online March 20, 2020

Chalcogenide glass (ChG) waveguides with sub-micrometer widths are fabricated by a hot melt smoothing and micro-trench filling method using As_2S_7 glass and their properties on nonlinear optics are investigated. The third-order nonlinear optical property is measured by the experiment of stimulated four-wave mixing, showing a nonlinear coefficient of 14.1 $W^{-1}m^{-1}$. Stimulated Brillouin scattering amplification is also demonstrated in the waveguide sample. The measured Brillouin shift and Brillouin gain coefficient are 6.25 GHz and 377 W^{-1} m^{-1}, respectively. The experiment results show that the ChG waveguides fabricated by this method have high quality and good performance on optical nonlinearity.

Chalcogenide glass (ChG) waveguides have large Kerr nonlinearity as well as low two-photon absorption and free-carrier absorption,[1,2] which are preferred in applications of nonlinear optics such as supercontinuum generation,[3–5] all-optical signal processing[6] and photon pair generation.[7] On the other hand, because of the relatively high refractive index and low sound velocity in ChG materials, both optical and acoustic modes can be confined in the ChG core of the waveguides,[8] providing a good platform for integrated stimulated Brillouin scattering (SBS).[9,10] However, the fabrication of on-chip ChG waveguides with high quality is not easy due to the unique mechanical and thermal properties of ChG materials.[11] Usually, the first step of ChG waveguide fabrication is to deposit ChG films onto the substrates by thermal evaporation[12] or sputtering.[13] Then, the patterns of waveguides are determined on the ChG films by lithography, following by etching[14] or lift-off process[15] to fabricate the waveguides. However, the alkaline developer used in these processes may react to the ChG films and reduce the quality of fabricated waveguides.[16] Hence, extra steps are required to protect the ChG films during lithography and etching processes,[17,18] which makes the fabrication procedure complex and difficult to handle. Recently, several new fabrication methods such as the solution-based method[19] and nanoimprinting[20] are developed to fabricate ChG waveguides. However, the residual organic solution in the solution-based method may cause high transmission loss,[21] and the fabrication process of nanoimprinting requires specialized equipment and precise experimental condition control.[22,23]

In our previous work, we proposed and demonstrated a fabrication method for on-chip integrated ChG devices based on the material properties of low melting temperature and good flowability when they are melted.[24] The waveguide structures were realized by melting the ChG films and making ChG materials fill into micro-trenches. This method avoids lithography, etching or lift-off processes on the ChG films, providing a simple way to realize high quality ChG waveguides. In this work, we fabricate long ChG waveguides by this method and measure their properties on nonlinear optics, including third-order nonlinear coefficient and Brillouin gain coefficient.

The fabrication process of the long ChG waveguide samples is similar to our previous work.[24] Firstly, micro-trenches are fabricated on the silica substrate by electron beam lithography (EBL) and inductively coupled plasma etching. Here, EBL replaces photolithography in the previous work since narrower waveguides are preferred to improve the nonlinear optical properties. After the etching process, the chip is dipped into buffered hydrofluoric acid for a few seconds to reduce sidewall roughness. Then, a thin ChG film is deposited onto the substrate by thermal evaporation. After film deposition, the chip is heated to 180 °C on a hot plate and the ChG film is melted in N_2 atmosphere to avoid oxidation. During the melting process, the ChG material fills into micro-trenches with a flat upper surface due to the self-smoothing effect. By this way, a reverse ridge ChG waveguide is formed on the silica substrate. The ChG material we choose in this experiment is As_2S_7 due to the low melting temperature and good flowability when it is melted. This fabrication method could also be applied to other ChG materials with good flowability if the heating processes are controlled precisely.

Figure 1(a) shows the scanning electron microscope (SEM) picture of the cross section of a typical waveguide sample. The width and depth of the micro-trench are 910 nm and 370 nm, respectively, and the thickness of As_2S_7 film out of the micro-trench is 320 nm. It can be seen that the As_2S_7 glass fills into the micro-trench in the heating process and the upper surface of As_2S_7 film is flat due to the self-smoothing effect. The inset picture shows the simulated electric field profile of the fundamental quasi-TE mode in the waveguide at 1550 nm. The refractive index of As_2S_7 glass used in the calculation is 2.22, which is measured by an ellipsometer. It can be seen that the electric field is well confined by the reverse ridge structure. The effective area (A_{eff}) of the fundamental quasi-TE mode is calculated to be 0.72 μm^2 using the expression of $A_{\mathrm{eff}} = \frac{\left(\iint |F(x,y)|^2\, dxdy\right)^2}{\iint |F(x,y)|^4\, dxdy}$, where $F(x, y)$ is the transverse electric field of the mode.[25]

Waveguide samples with different lengths are fabricated. The probe light at 1550 nm is coupled into and out of the waveguide by two lensed fibers, and the insertion losses of

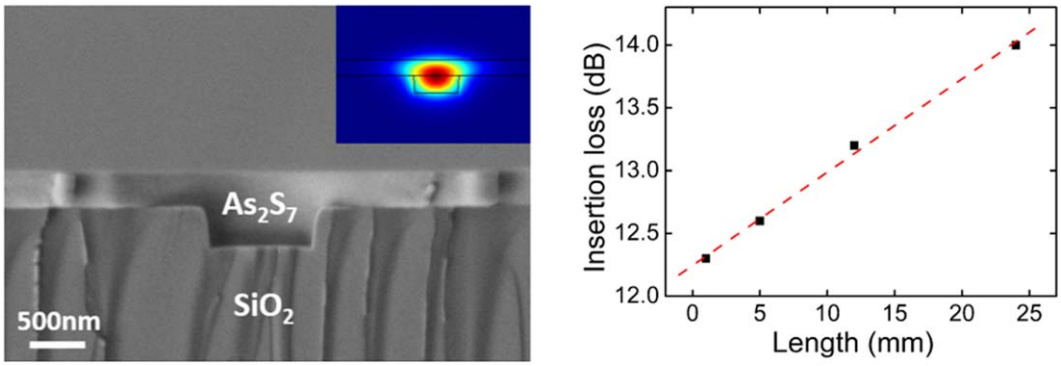

Fig. 1. (Color online) (a) The SEM picture of the cross section of a typical waveguide sample. The inset is the simulated electric field profile of the fundamental quasi-TE mode in the waveguide. (b) Measured results of the insertion losses of the fundamental quasi-TE mode in waveguides with different lengths. The red line is the linear fitting line, indicating an attenuation of 0.74 dB cm^{-1}.

the fundamental quasi-TE mode in waveguides with different lengths are measured. The results are plotted in Fig. 1(b), and the red line in the figure is the linear fitting result. It can be seen that the attenuation of the fundamental quasi-TE mode in these waveguides is 0.74 dB cm^{-1}, showing their good transmission property. Since the optical loss of As-S glass material is relatively low in the telecom band,[26] the sidewall roughness of silica micro-trenches is the main cause of waveguide attenuation, which can be improved by better etching process of the silica substrate. The fundamental quasi-TM mode is also supported in this waveguide, but the transmission loss is higher than the fundamental quasi-TE mode. Meanwhile, the simulation also shows that no higher-order mode is supported in the waveguide sample. Hence, in the following measurement, only the fundamental quasi-TE mode is considered.

The third-order nonlinear coefficient of these ChG waveguides is measured by the experiment of stimulated four-wave mixing (FWM). The waveguide sample used in the experiment is 5.7 cm in length, with an insertion loss of 18.6 dB. According to the measured waveguide attenuation in Fig. 1(b), it can be estimated that the transmission loss of the sample is about 4.2 dB and the coupling loss is about 7.2 dB/facet. The experimental setup of stimulated FWM is shown in Fig. 2(a). The pump and signal lights are generated from two CW tunable lasers, respectively. The pump light is amplified by an Erbium-doped fiber amplifier (EDFA) before it is combined with the signal light. A set of optical filters are used to filter out the amplified spontaneous emission of the EDFA and the lights generated by nonlinear processes in optical fibers. Then, the pump and signal lights are injected into the waveguide sample. An optical spectrum analyzer (OSA) is used to measure the output lights from the waveguide. In the experiment, an idler light with a frequency of $\omega_{\text{idler}} = 2\omega_{\text{pump}} - \omega_{\text{signal}}$ is generated by stimulated FWM and observed by the OSA. To demonstrate that the idler light is generated in the waveguide sample, an experiment for comparison is carried out, in which the input and output lensed fibers are coupled with each other directly. The insertion loss is adjusted to the same value as that with the ChG waveguide sample by tuning the space between them. In this case, no idler light is observed, indicating that stimulated FWM is generated in the waveguide sample, and the impact of nonlinear processes in optical fibers in the setup can be neglected. On the other hand, it is well known that the bandwidth and conversion efficiency of stimulated FWM are influenced by the phase match condition among the pump, signal and idler lights, which is related to the waveguide dispersion. To show the phase match condition in FWM process, the group velocity dispersion (GVD) parameter $D = -\frac{2\pi c}{\lambda^2}\frac{d^2\beta}{d\omega^2}$ is calculated, and the results are plotted in Fig. 2(b). It can be seen that the waveguide has normal dispersion in the telecom band, with a peak GVD of −130 ps/nm/km at 1.6 μm, and the calculated conversion bandwidth is ∼15 nm under the experimental condition. Then, the conversion efficiency of FWM process under different wavelength spaces between the pump and signal lights is measured experimentally. Here, the conversion efficiency is defined as $\eta = \frac{P_i(L)}{P_s(0)}$, i.e. the power ratio of the idler light at the output of waveguide to the input signal light. In the experiment, the pump wavelength and coupled power of pump light are set as 1550 nm and 10.8 dBm, respectively, and the coupled signal power is lower than −5 dBm, ensuring that it can be treated as a small signal in the stimulated FWM process. The results are shown in Fig. 2(c). It can be seen that the 3 dB bandwidth of the stimulated FWM process in the waveguide is ∼20 nm. The small bandwidth difference between the experiment result and calculation may be due to the imprecise refractive index of As_2S_7 used in the calculation, which is measured by an ellipsometer on another As_2S_7 film sample.

In order to measure the third-order nonlinear coefficient γ, input pump light with different power levels are injected into the waveguide. Under a small pump/signal wavelength space, the power of idler light at the output end of the waveguide can be calculated by $P_i = (\gamma P_p L_{\text{eff}})^2 P_s \cdot e^{-\alpha L}$, where α is the attenuation coefficient of the waveguide, L is the waveguide length, P_p and P_s are the powers of pump light and signal light coupled into the waveguide, respectively, and $L_{\text{eff}} = (1 - e^{-\alpha L})/\alpha$ is the effective length of the waveguide.[27] Figure 2(d) shows the measured FWM conversion efficiency under different pump power levels with a pump/signal wavelength space of 3 nm, and the third-order nonlinear coefficient can be obtained by linear fitting in the log scale, which is $\gamma = 14.1\ W^{-1}\ m^{-1}$. This value is at the same level as the third-order nonlinear coefficients of reported high quality As_2S_3 waveguides fabricated by traditional methods.[28,29] The nonlinear index of the As_2S_7 glass can be estimated as $n_2 = 2.5 \times 10^{-18}\ m^2\,W^{-1}$ according to

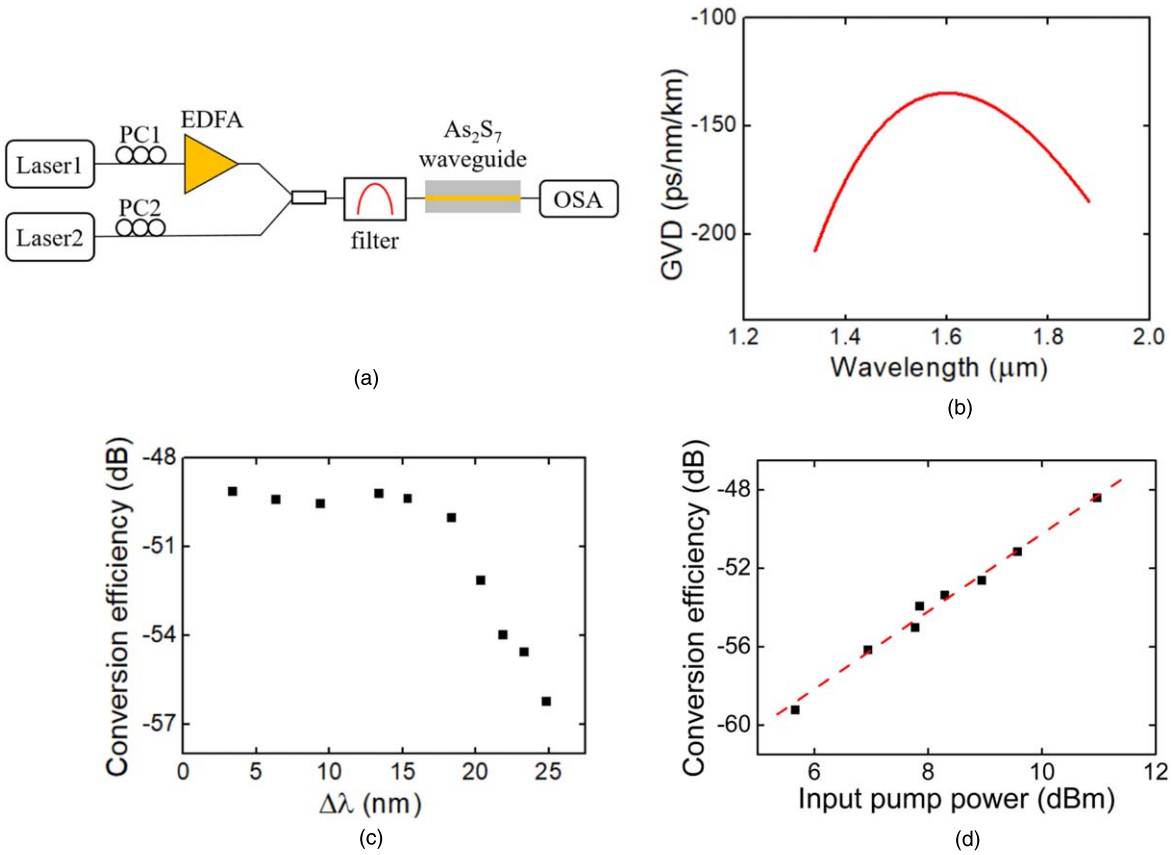

Fig. 2. (Color online) (a) Experimental setup of stimulated FWM in the ChG waveguide sample. The pump light is amplified by an EDFA, then combined with the signal light and injected into the As_2S_7 waveguide. The output light is measured by an OSA. (b) Simulation result of group velocity dispersion (GVD) versus wavelength. (c) FWM conversion efficiency under different wavelength spaces between pump and signal lights under a coupled pump power of 10.8 dBm at 1550 nm. (d) FWM conversion efficiency under different coupled pump power levels with a pump/signal wavelength space of 3 nm.

$\gamma = n_2\omega_p/cA_{\text{eff}}$,[30] where ω_p is the angular frequency of pump wave and A_{eff} is the effective mode area of the fundamental quasi-TE mode [0.72 μm^2 according to the calculation shown in Fig. 1(a)].

Besides their good third-order nonlinearity, ChG waveguides are also preferred to realize on-chip SBS. Since the sound velocities of As-S materials with different compositions are close to each other,[26] we can estimate the SBS property of the fabricated waveguide sample by the sound velocity of As_2S_6 glass, which is ~2360 m s^{-1}, far lower than the sound velocity in the silica substrate (5960 m s^{-1}).[26,31] Hence, it can be expected that the acoustic waves can also be confined in the waveguide, leading to on-chip SBS with high efficiency. The Brillouin shift of the waveguide is estimated to be 6.05 GHz according to $\nu_B = 2n_p v_a/\lambda_p$, where n_p is the effective refractive index of the optical mode, v_a is the sound velocity in the material and λ_p is the wavelength of pump light.

Figure 3(a) is the experimental setup for the measurement of Brillouin gain coefficient in the fabricated waveguide samples. The pump light is generated by a telecom band laser, with a wavelength of 1552.5 nm. It is amplified by an EDFA and then coupled into the waveguide sample from the left end through a circulator and a lensed fiber. The probe light is generated by another narrow-linewidth tunable laser and injected into the waveguide sample from the right end by another lensed fiber. When the probe light propagates along the waveguide, it would experience the amplification by SBS if its frequency is lower than the frequency of pump light with a specific frequency difference, which is the Brillouin shift. The amplified probe light outputted from the left end of the waveguide is measured by heterodyne detection after it passes through the circulator and an optical filter. The optical filter is used to eliminate the reflected pump light from the end surface of the waveguide sample. The optical local oscillator in the heterodyne detection is extracted from the pump light before it is amplified by the EDFA. A high-speed photodetector and an electrical spectrum analyzer are used to realize the heterodyne detection. In the experiment, the frequency of probe light is tuned to measure the probe amplification under different frequency spaces between the pump and probe light. A typical result is shown in Fig. 3(b), which is measured under a coupled pump power of 18.3 dBm. The power of the input probe light is lower than 0 dBm, ensuring that it is a small signal in the Brillouin amplification process. It can be seen that the signal is obviously amplified when the frequency difference between the pump and signal lights is around 6.25 GHz, which is close to the estimated Brillouin shift (6.05 GHz). The red curve is the result of Lorentzian fitting, showing a FWHM of 150 MHz, which is relatively large compared to some reported results of SBS in ChG waveguides.[9,32] It may be due to the open boundary of acoustic wave on the upper surface of As_2S_7 film, which could cause acoustic wave leakage into the upper As_2S_7 film out of the micro-trench. Numerical simulations show that applying a silica upper-cladding on the As_2S_7 film would provide better acoustic confinement, and the Brillouin gain would also increase

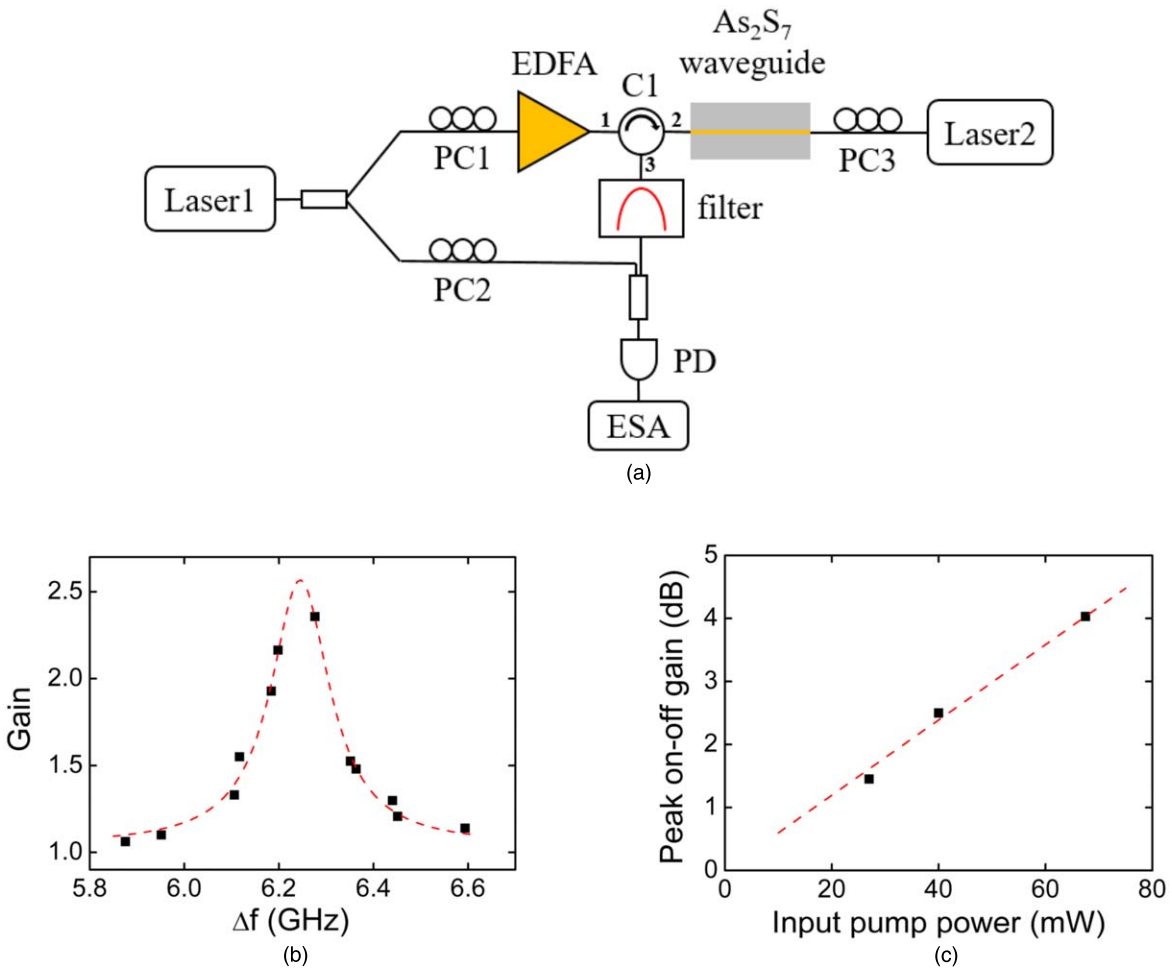

Fig. 3. (Color online) (a) Experimental setup for the measurement of Brillouin gain coefficient. (b) Measured Brillouin gain spectrum and the result of Lorentzian fitting. (c) Peak on–off gains of the probe light under different pump power coupled into the waveguide sample.

because of the higher overlap between the acoustic and optical modes.[33] On the other hand, reducing the thickness of the upper As_2S_7 film is also an effective way to make the acoustic mode more confined in the micro-trench structure.

The amplification of probe light can be indicated by the on–off gain due to SBS in the waveguide, which is denoted by G_{on-off}. According to the theory of SBS, the small signal on–off gain can be calculated by $G_{on\text{-}off}\,(\text{in dB}) = 4.343 G_B P_0 L_{eff}$, where G_B is the Brillouin gain coefficient, P_0 is the pump power and L_{eff} is the effective length of the waveguide.[31] To obtain the Brillouin gain coefficient G_B of the waveguide sample, on–off gains of the probe light under different pump power levels are measured and plotted in Fig. 3(c). The red line is the linear fitting result, which indicates that the measured Brillouin gain coefficient is $G_B = 377\ \text{W}^{-1}\ \text{m}^{-1}$, using $L_{eff} = 3.65$ cm in the calculation. This value is comparable with reported As_2S_3 glass waveguides and suspended silicon waveguides for Brillouin scattering.[34,35]

In conclusion, we fabricated high quality As_2S_7 glass waveguides by the hot melt smoothing and micro-trench filling method and investigated their nonlinear optical properties. The transmission property of the fabricated waveguide samples with sub-micrometer widths are measured by cut-back method, showing a low attenuation of 0.74 dB cm^{-1} for the fundamental quasi-TE mode. The third-order nonlinear optical property is demonstrated by stimulated FWM in a waveguide sample of 5.7 cm in length. The experiment results show that the third-order nonlinear coefficient γ is 14.1 $\text{W}^{-1}\ \text{m}^{-1}$. SBS amplification is also demonstrated in the waveguide sample. The Brillouin gain spectrum is obtained by a pump-probe method. The measured Brillouin shift and FWHM of the Brillouin gain spectrum are 6.25 GHz and 150 MHz, respectively. By the measurement of on–off gains of the probe light under different pump power levels, the Brillouin gain coefficient of the waveguide sample is obtained, which is 377 $\text{W}^{-1}\ \text{m}^{-1}$. These experiment results show that the waveguides fabricated by the hot melt smoothing and micro-trench filling method have high quality and good performance on optical nonlinearity, which have great potential in developing integrated nonlinear optical devices.

Acknowledgments This work was supported by National Key R&D Program of China under Contract No. 2018YFB2200400 and 2017YFA0303704; National Natural Science Foundation of China under Contract No. 61875101, 61575102 and 61621064; Beijing National Science Foundation under Contract No. Z180012; Beijing Academy of Quantum Information Sciences under Contract No. Y18G26; Tsinghua University Initiative Scientific Research Program.

ORCID iDs Wei Zhang https://orcid.org/0000-0002-6848-6807

1) T. Wang, X. Gai, W. Wei, R. Wang, Z. Yang, X. Shen, S. Madden, and B. Luther-Davies, Opt. Mater. Express **4**, 1011 (2014).
2) M. Asobe, T. Kanamori, K. Naganuma, H. Itoh, and T. Kaino, J. Appl. Phys. **77**, 5518 (1995).

3) Y. Yu, X. Gai, P. Ma, K. Vu, Z. Yang, R. Wang, D.-Y. Choi, S. Madden, and B. Luther-Davies, Opt. Lett. **41**, 958 (2016).
4) J.-É. Tremblay, M. Malinowski, K. A. Richardson, S. Fathpour, and M. C. Wu, Opt. Express **26**, 21358 (2018).
5) Q. Du, Z. Luo, H. Zhong, Y. Zhang, Y. Huang, T. Du, W. Zhang, T. Gu, and J. Hu, Photonics Res. **6**, 506 (2018).
6) B. J. Eggleton, T. D. Vo, R. Pant, J. Schr, M. D. Pelusi, D. Yong Choi, S. J. Madden, and B. Luther-Davies, Laser Photonics Rev. **6**, 97 (2012).
7) M. J. Collins et al., Opt. Lett. **37**, 3393 (2012).
8) C. G. Poulton, R. Pant, and B. J. Eggleton, J. Opt. Soc. Am. B **30**, 2657 (2013).
9) R. Pant, C. G. Poulton, D.-Y. Choi, H. Mcfarlane, S. Hile, E. Li, L. Thevenaz, B. Luther-Davies, S. J. Madden, and B. J. Eggleton, Opt. Express **19**, 8285 (2011).
10) M. Merklein, I. V. Kabakova, T. F. S. Büttner, D. Y. Choi, B. Luther-Davies, S. J. Madden, and B. J. Eggleton, Nat. Commun. **6**, 1 (2015).
11) B. J. Eggleton, B. Luther-Davies, and K. Richardson, Nat. Photonics **5**, 141 (2011).
12) J.-F. Viens, C. Meneghini, A. Villeneuve, T. V. Galstian, and É. J. Knystautas, J. Lightwave Technol. **17**, 1184 (1999).
13) F. Verger et al., Opt. Mater. Express **3**, 2112 (2013).
14) X. Gai, D.-Y. Choi, S. Madden, and B. Luther-Davies, Opt. Express **20**, 13513 (2012).
15) H. Lin et al., Opt. Lett. **38**, 1470 (2013).
16) D. Y. Choi, S. Madden, A. Rode, R. Wang, D. Bulla, and B. Luther-Davies, J. Non-Cryst. Solids **354**, 5253 (2008).
17) D. Y. Choi, S. Madden, D. Bulla, A. Rode, R. Wang, and B. Luther-Davies, Phys. Status Solidi c **8**, 3183 (2011).
18) X. Xia, Q. Chen, C. Tsay, C. B. Arnold, and C. K. Madsen, Opt. Lett. **35**, 3228 (2010).
19) Y. Zha, P. T. Lin, L. Kimerling, A. Agarwal, and C. B. Arnold, ACS Photonics **1**, 153 (2014).
20) Y. Zou et al., Adv. Opt. Mater. **2**, 478 (2014).
21) Y. Zou et al., Adv. Opt. Mater. **2**, 759 (2014).
22) D. Yehuda, E. Kassis, S. Joseph, and M. Schvartzman, J. Vac. Sci. Technol. B **36**, 031602 (2018).
23) T. Y. Yan, X. Shen, R. P. Wang, G. X. Wang, S. X. Dai, T. F. Xu, and Q. H. Nie, Chin. Phys. B **26**, 024213 (2017).
24) Y. Zhai, R. Qi, C. Yuan, W. Zhang, and Y. Huang, Appl. Phys. Express **9**, 052201 (2016).
25) C. Koos, L. Jacome, C. Poulton, J. Leuthold, and W. Freude, Opt. Express **15**, 5976 (2007).
26) I. I. Shpak, R. M. Evich, Z. P. Gad'mashi, S. I. Perechinskii, Y. M. Vysochanskii, and V. Y. Slivka, J. Appl. Spectrosc. **71**, 902 (2004).
27) K. O. Hill, D. C. Johnson, B. S. Kawasaki, and R. I. MacDonald, J. Appl. Phys. **49**, 5098 (1978).
28) M. R. Lamont, B. Luther-Davies, D.-Y. Choi, S. Madden, and B. J. Eggleton, Opt. Express **16**, 14938 (2008).
29) C. Xiong et al., Appl. Phys. Lett. **98**, 051101 (2011).
30) C. Xiong, L. G. Helt, A. C. Judge, G. D. Marshall, M. J. Steel, J. E. Sipe, and B. J. Eggleton, Opt. Express **18**, 16206 (2010).
31) B. J. Eggleton, C. G. Poulton, and R. Pant, Adv. Opt. Photonics **5**, 536 (2013).
32) A. Zarifi et al., Opt. Lett. **43**, 3493 (2018).
33) S. R. Mirnaziry, C. Wolff, M. J. Steel, B. J. Eggleton, and C. G. Poulton, Opt. Express **24**, 4786 (2016).
34) I. V. Kabakova, R. Pant, D.-Y. Choi, S. Debbarma, B. Luther-Davies, S. J. Madden, and B. J. Eggleton, Opt. Lett. **38**, 3208 (2013).
35) N. T. Otterstrom, E. A. Kittlaus, S. Gertler, R. O. Behunin, A. L. Lentine, and P. T. Rakich, Optica **6**, 1117 (2019).